

Autonomous

12. Autonomous Underwater Gliders

Scott A. Jenkins, Gerald D'Spain

This chapter discusses the characteristics, design considerations, and performance of autonomous underwater (UW) gliders. These buoyancy-propelled, winged vehicles can be categorized as: (1) *profiling gliders* that traverse in bobbing trajectories to collect vertical profiles of ocean properties and (2) *cross-country gliders* designed for point-to-point horizontal transport efficiency. Horizontal transport efficiency is quantified by net transport economy and specific energy consumption. The latter metric for a glider is equal to its inverse lift-to-drag ratio (also called *finesse*) and is equivalent to the glide slope in steady-state, nonturning glides. Increases in efficiency can be obtained by:

1. Increasing the loaded mass (with larger buoyancy engines) and increasing the overall size of the glider, which increases the glider's speed and maintain sufficiently high Reynold's numbers to avoid the drag crisis.
2. Reducing the ratio of the total vehicle wetted area to wing area, via use of flying wing or blended wing body shapes, and
3. Increasing the wing aspect ratio, within structural strength and stiffness limitations.

Gliders have an intrinsic advantage in transport efficiency over conventional prop-driven autonomous underwater vehicles (AUVs) due to the simpler vortex dynamics of a wing versus a propeller. As a result, gliders can fly cooperatively

12.1	Concept	301
12.2	Hydrodynamics of Wings Versus Propellers	305
12.3	Underwater Glider Attributes and Limitations	306
	12.3.1 Depth Unlimited Roaming.....	307
	12.3.2 Depth Limited Roaming.....	307
	12.3.3 2-D Station Keeping.....	307
	12.3.4 Payload/Cargo Delivery.....	307
	12.3.5 Level Flight Hybrids.....	307
12.4	Optimal Size and Shape for Horizontal Transport Efficiency	308
	12.4.1 Net Transport Economy	308
	12.4.2 Size Factors.....	310
	12.4.3 Shape Factors.....	311
	12.4.4 Glide Polar	313
12.5	Thermal Glider	318
12.6	Discussion and Conclusions	319
	References	320

with other winged vehicles or employ multielement wings to further improve transport efficiency. Although a glider must change depth to move forward, these depth changes not only allow the collection of vertical profiles of ocean properties, but also enable the extraction of energy from the ocean's vertical temperature gradients (*thermal glider*).

12.1 Concept

The underwater (UW) glider is a buoyancy-propelled, winged vehicle, analogous to a glider in air. The mechanical power of locomotion needed to overcome the drag on the vehicle as it moves through a fluid medium is supplied by gravity in the form of net buoyancy (positive or negative). Horizontal motion using the vertical force of gravity is made possible by the action of lift produced by a wing that acts perpendicular to the trajectory of the vehicle. Therefore, horizontal translation

only occurs when the flight path is inclined at a glide angle (Fig. 12.1) that deviates from the horizontal plane in the direction of the vertical net force of gravity (upward for a positive net buoyancy and downward for negative net buoyancy). Inclination of the flight path along some glide angle allows the net hydrodynamic force of lift and drag to balance the net buoyancy in steady-state flight. The inclined flight path that produces this force balance also gives rise to a net vertical motion.

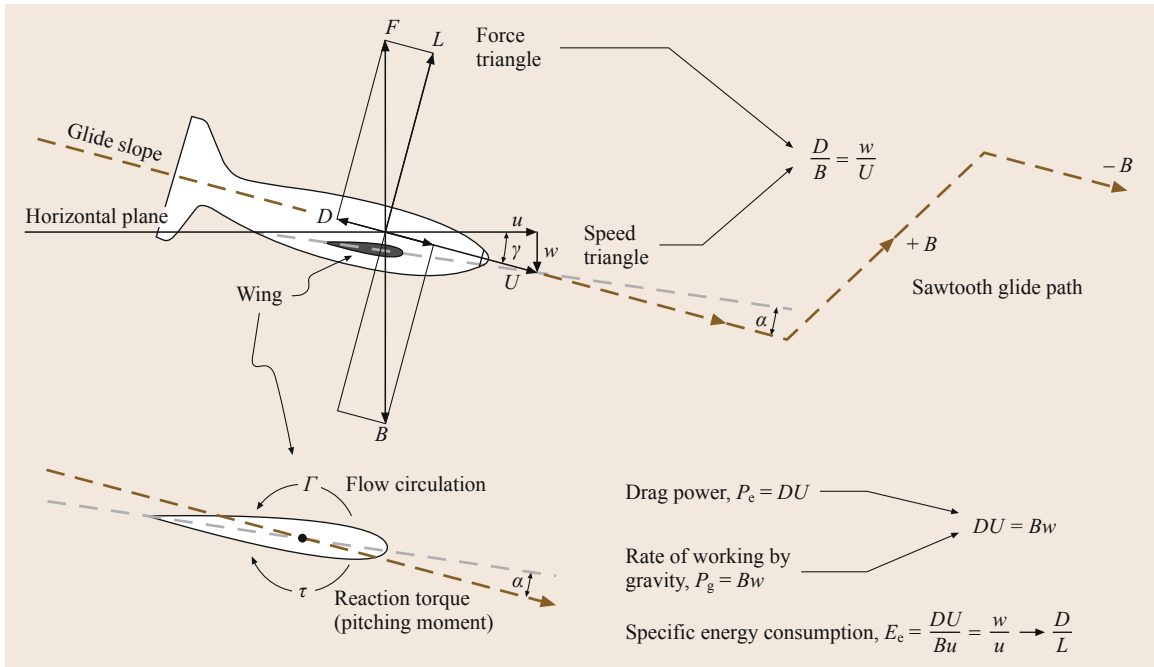


Fig. 12.1 Force balance and energetics for sawtooth glide path (after [12.1]). B = net buoyancy, L = lift, D = drag, F = resultant of lift and drag, u = horizontal speed, w = vertical speed, U = glide speed = magnitude of resultant of horizontal and vertical velocity, Γ = flow circulation, τ = pitching moment that is a reaction torque to the flow circulation, γ = glide angle from the horizontal, α = angle of attack, $\gamma - \alpha$ = pitch angle

Although analogous, a few differences do exist between air and underwater gliders. First, whereas an airborne glider only executes descending glides, and therefore must create lift only in the upward direction, a UW glider flies ascending as well as descending glides. In order to change the buoyancy between descending and ascending glides, a UW glider must be equipped with a buoyancy engine (Fig. 12.2) that effectively changes the displaced volume of the glider (equivalent to a change in average density for constant mass). This requirement to change the direction of lift – from upward on descending glides to downward on ascending glides – places constraints on the wing design (fixed camber usually is not designed into the wings of UW

gliders) and additional demands on vehicle flight control. It also results in some interesting effects; for example, to turn to starboard, an ascending glider must bank to port, opposite the direction of a descending glider. These changes in buoyancy for an underwater glider occur about the point of neutral buoyancy, where the dry bulk weight is balanced by the weight of the water displaced by the vehicle. Therefore, the weight of an UW glider’s loaded mass (its net buoyancy) can be remarkably different than its dry bulk weight, whereas these two weights are nearly the same for platforms in air. Another difference in flying in air versus underwater is the stability of the fluid medium. The troposphere, the lowermost 10 km of the earth’s atmosphere, is a convective boundary layer with warmer, less dense air underlying colder, denser air. The resulting convective overturn causes turbulence which can make controlled flight very challenging. In contrast, the ocean is stably stratified for the most part, so that once an UW glider is traveling on its desired heading, very little additional flight control is required.

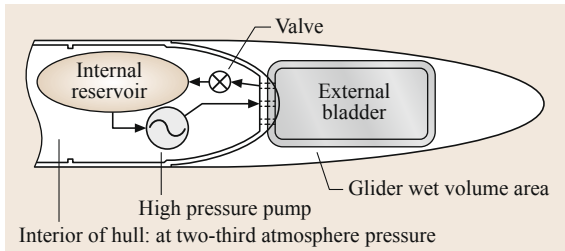


Fig. 12.2 Closed-loop oil-based buoyancy engine (after [12.2])

Underwater gliders originated in the early 1960s with the *Concept Whisper*, a prototype 2-man swimmer delivery vehicle (SDV) built by General Dynamics Corporation [12.5]. A prototype of *Concept Whisper* was built and tested in shallow dives in San Diego Bay in 1964. *Concept Whisper* was a classified project

and for several decades, nothing of its concepts and testing was known to the outside world. In the 1970s, analysis of the energetics of UW gliders and an evaluation of various applications was performed at the Naval Electronics Laboratory. At the end of the 1980s, *Stommel* independently proposed a fleet of autonomous gliders referred to as *Slocums* to profile the ocean's water properties [12.6]. Shortly thereafter, underwater gliders started being developed into useful sensor platforms as a result of sustained funding from the Office of Naval Research. These underwater gliders were developed and tested primarily for the purpose of profiling ocean water properties, commensurate with the role first envisioned by *Stommel* [12.6], and so are referred to herein as *profiling gliders* (Fig. 12.3).

The profiling gliders include *Spray*, *Seaglider*, and *Slocum* [12.2–4]. All three designs are based on a conventional winged body of revolution. Emphasis was placed on optimizing the performance of the profiling gliders to travel up and down through the water column at steep glide angles to obtain vertical profiles of water mass properties, rather than optimizing for cross-country performance as with conventional gliders in air. The profiling gliders also were designed to accommodate the limited deck space available on small oceanographic vessels, and be two-person portable. As a result, all are similar in size and weight; order 2 m in length, 1 m in wingspan, 50 L in total vehicle volume, and operating at a net buoyancy of about 1–3 N. These three types of UW gliders have logged hundreds of at-sea days during a given mission, collecting ocean profiles. When running *down-wind* with western boundary currents such

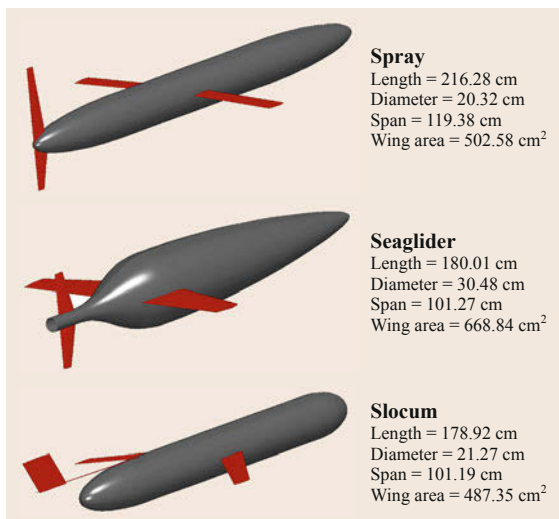


Fig. 12.3 Profiling underwater gliders, post *Concept Whisper*. Developed for vertical profiling of ocean water mass properties (after [12.2–4])

as the Kuroshio or Gulf Stream Currents, they have covered distances of 1000 km and more.

In the latter half of the 2000s, another type of UW glider, referred to as *cross-country gliders*, was developed for long horizontal range, long duration missions of passive ocean monitoring. These gliders have

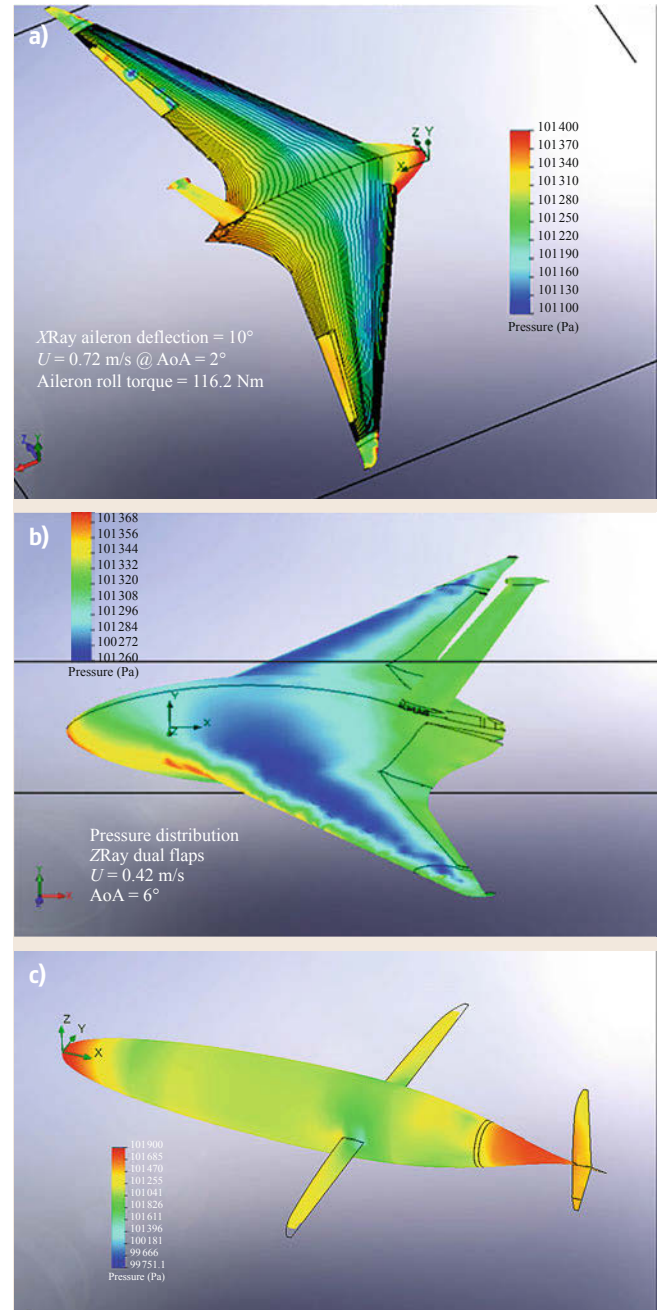


Fig. 12.4a–c Cross-country underwater gliders: Liberdade/XRay (a), Liberdade/ZRay (b), winged body of revolution (c)

larger payload and cargo-carrying capacity, and emphasize point-to-point, *cross-country*, transport efficiency. Various designs of these new cross-country gliders have been built and are currently undergoing sea trials, including two examples of flying wings, the Liberdade/XRay and Liberdade/ZRay gliders (Fig. 12.4). The XRay and ZRay designs use a seawater-based buoyancy engine analogous to the ballast system on submarines, while other cross-country glider designs use larger versions of the type of oil-based buoyancy engine diagrammed in Fig. 12.2.

As discussed earlier, underwater gliding is a buoyancy driven form of locomotion in which the power needed to overcome the drag (D) on the vehicle as it moves at a speed U through water is supplied by gravity in the form of positive or negative net buoyancy ($+/-B$). Horizontal translation using the vertical force of gravity is made possible by the lift (L) produced by a wing that acts perpendicular to the trajectory of the vehicle. Inclination of the glide slope from the horizontal gives rise to a horizontal component of lift that provides the force of forward propulsion. In steady-state flight, this force is balanced by the horizontal component of the drag, which yields the relationship that the glide slope is equal to the inverse of the lift-to-drag ratio. The lift-to-drag ratio (L/D) of a wing is also referred to as its *finesse* [12.7]. In the vertical direction, inclination of the glide slope from the horizontal also allows the net hydrodynamic force of lift and drag (F) to balance the net buoyancy in steady-state flight, but implies that a net vertical motion will result, (Fig. 12.1). This vertical motion is referred to as the sink rate (w). During each of the descending or ascending slopes of the sawtooth glide path, the power needed to overcome drag ($P_e = DU$) is equal to the rate of work by gravity acting down (or up) ($P_g = Bw$). Thus

$$P_g = P_e = DU = Bw . \quad (12.1)$$

Because the force triangle and the speed triangle in Fig. 12.1 are proportional, the power expenditure per horizontal distance traveled scales in direct proportion to the glide slope ($w/u \approx D/L$), or inversely with the lift-to-drag ratio (L/D). Therefore, by imparting the underwater glider with low drag and high lift properties, its energy consumed to produce locomotion in the horizontal direction can be minimized. In other words, almost all the energy in forward propulsion is consumed at the bottom of the dive cycle where the glider's displaced volume must be increased against ambient pressure. By decreasing the glide slope, i. e., increasing L/D , the number of times this change in displaced volume must occur is minimized for a given horizontal distance traveled.

The *buoyancy engine* generates a variable displaced volume increment, or net buoyancy volume $\pm V_b$; such that the total displaced volume of the glider is $V_d = V_s \pm V_b$, where V_s represents the volume of the glider's rigid body. By varying the net buoyancy volume, the buoyancy engine causes the net buoyancy force to alternate between positive and negative states, $B = \pm \rho g V_b$. Typically, the underwater glider is trimmed to be approximately neutrally buoyant in seawater when $V_b = 0$; so that the average density of the glider approaches the ambient seawater density, $\bar{\rho}_s \rightarrow \rho$, and the net buoyancy reduces to $B = \rho g (V_d - V_s) = 0$. In addition to the volume of the glider's rigid body and buoyancy engine displacement volume, the total volume of the vehicle, V_0 , also includes void-space water V_{void} , that enters into the freely flooding internal spaces. Thus, the total volume of the vehicle is represented by: $V_0 = V_s \pm V_b + V_{\text{void}}$. Because the total vehicle volume is fixed, the void water is a function of the net buoyancy volume, $V_{\text{void}} = f(V_b)$, and the hull must accommodate ventilation of the void water with the outside water. Under neutral buoyancy, the total vehicle mass becomes $M_0 = \rho (V_s \pm V_b + V_{\text{void}})$. A variety of buoyancy engine technologies have been employed, including closed-loop liquid-based engines [12.2–4] for which buoyancy engine capacity is in the neighborhood of $0.1\% \leq V_b/V_0 \leq 4\%$; open-loop seawater-based buoyancy engines, as with XRay and ZRay having capacities typically ranging from $1\% \leq V_b/V_0 \leq 8\%$; open-loop compressed gas-based systems [12.8] having $5\% \leq V_b/V_0 \leq 20\%$; as well as the open-loop gas-based buoyancy engines that consume gas-generating compounds, such as those used in Concept Whisper [12.5] for which $11\% \leq V_b/V_0 \leq 28\%$. The profiling gliders use a closed-loop oil-based buoyancy engine as diagrammed in Fig. 12.2, while the cross-country gliders typically use open-loop seawater-based buoyancy engines. The closed-loop liquid-based engines have the disadvantage that the weight of the working fluid (oil) is always onboard, limiting the net buoyancy capacity to about half that of an open circuit buoyancy engine that uses seawater (e.g., as in a submarine buoyancy system). Also, oils can undergo phase changes from liquid to vapor under large decreases in pressure, which can occur in a closed-loop system when the oil is transferred from the external bladder to the internal reservoir to initiate ascent from deep depths. This phase change phenomenon limits the ability to evacuate all of the oil in the external bladder. Regardless, both close- and open-loop buoyancy engines typically are driven by small electric pumps that produce only low levels of intermittent self-noise, ideally suited for passive underwater monitoring applications or those requiring stealthy behavior.

12.2 Hydrodynamics of Wings Versus Propellers

Buoyancy-propelled winged vehicles are intrinsically more efficient than propeller-driven vehicles because the power needed to overcome drag (P_e) is minimized by the simplicity of the vortex system of the wing (Fig. 12.5). From the first law of thermodynamics, P_e is given by the rate of dissipation of the flow kinetic energy as a consequence of the generation of vorticity $\boldsymbol{\Omega} = \nabla \times \mathbf{u}$. On a winged vehicle, the preponderance of vorticity is generated during the action of making lift. From [12.11], P_e is given by

$$P_e = \iiint \mu (\boldsymbol{\Omega} \cdot \boldsymbol{\Omega}) dx dy dz, \quad (12.2)$$

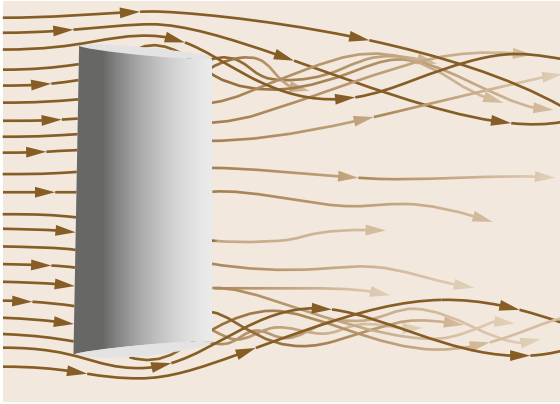


Fig. 12.5 Flow visualization shows the trailing line vortices shed from the wing tips of a constant chord wing as viewed from the top looking downward (after [12.9]). Flow is from left to right

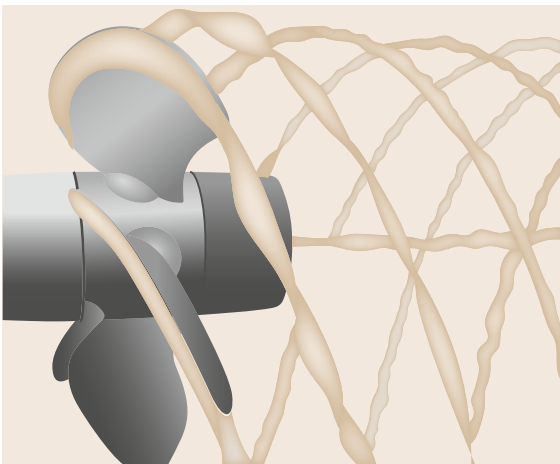


Fig. 12.6 Flow visualization of the trailing helical vortices shed from the tips of a propeller (after [12.9])

where (x, y, z) are the Cartesian coordinates fixed on the wing, with x being the horizontal coordinate in the chord-wise direction, y is the horizontal coordinate in the span-wise direction, and z is the vertical coordinate positive in the upward direction. The quantity μ is the dynamic viscosity, and the flow circulation, Γ , is related to the vorticity induced by a wing with vector airfoil sectional area \bar{A} according to $\Gamma = \int \boldsymbol{\Omega} \cdot d\bar{A}$. The vorticity released into the mean flow by a wing is at lowest order one-dimensional (1-D), in the form of a pair of trailing line-vortices shed from the wing tips (Fig. 12.5). In this case, the expression for the power needed to overcome drag reduces to

$$P_e = \mu \iiint \left[\left(\frac{\partial w}{\partial y} - \frac{\partial v}{\partial z} \right)^2 \right] dx dy dz \quad (\text{wing}), \quad (12.3)$$

where (u, v, w) are the components of fluid velocity in the (x, y, z) directions, respectively.



Fig. 12.7 The blue whale evolved winged tails (flukes), not propellers, for propulsion for their annual migrations over thousands of miles between feeding grounds and birthing grounds, as well as for endurance during high-speed pursuits from predators such as killer whales (after [12.10])

In contrast, a propeller is a rotating wing which releases the vorticity into the mean flow. It produces a more complex helical system of trailing vortices imparting swirl to the mean flow (Fig. 12.6). The trailing vortex system from a propeller is fully three dimensional; as a result, the power needed to overcome drag expression contains two additional terms

$$P_e = \mu \iiint \left[\left(\frac{\partial w}{\partial y} - \frac{\partial v}{\partial z} \right)^2 + \left(\frac{\partial u}{\partial z} - \frac{\partial w}{\partial x} \right)^2 + \left(\frac{\partial v}{\partial x} - \frac{\partial u}{\partial y} \right)^2 \right] dx dy dz \quad (\text{propeller}). \quad (12.4)$$

From the additional vorticity components in the vortex trail of a propeller comes higher dissipation rates that require greater expenditures of onboard power to maintain a given vehicle speed through the water, $U (= |\mathbf{u}|)$. The advantage in transport efficiency of a wing over a propeller in water is illustrated nature through the evolution of the propulsion systems for marine mammals, for example the blue whale (Fig. 12.7). Whales evolved winged tails (flukes) not propellers as the basis of their propulsion systems. Natural selection of winged tails did not occur for lack of a joint capable of 360° rotation, as the shoulder joint in primates clearly proves biomechanically viable.

12.3 Underwater Glider Attributes and Limitations

The most compelling attribute of an underwater glider from the point of view of other types of subsurface vehicles is its high endurance/long on-station time capability. This attribute arises because an UW glider can readily operate over its full flight envelope, from top speed to neutrally buoyant (determined by the net vehicle buoyancy created by its buoyancy engine). Therefore, it can conserve onboard propulsion energy by moving as slowly with respect to the surrounding medium as possible while still accomplishing its objectives. In addition, an UW glider has very low levels of self-noise (acoustically, electrically, and magnetically), because self-noise is created primarily by the buoyancy pump that is activated only episodically for short intervals. Once the underwater glider changes its net buoyancy, it can glide silently with no machinery or hydrodynamic noise until reaching the next reversal in the sawtooth glide path. (Again, the ocean's stable stratification minimizes disturbance from turbulence and so minimizes the need for actuating flight controls.) The intermittency of a glider's self-noise is in sharp contrast to the continuous self-noise emissions from propulsion of prop-driven vehicles. Finally, in contrast to prop-driven platforms, winged structures such as UW gliders can fly cooperatively to improve flight efficiency in horizontal transport. This point is illustrated later in this chapter.

The primary weakness of an UW glider compared with other types of underwater vehicles arises from its inability to maintain level flight in the water column – it must change depth to propel itself forward. This weakness actually is a strength when an objective is to collect vertical profiles of ocean properties.

As with all underwater vehicles, an UW glider is vulnerable to damage – from surface ship collisions,

harsh weather, and entanglement – while on the ocean surface. For missions that require covertness, the probability of platform detection is also much greater at the surface; all of a glider's stealthy attributes are compromised during surfacing periods. However, wideband, inexpensive (energy-wise, size and weight-wise, and cost-wise), two-way communications can be achieved only after surfacing. In addition, most environmental sources of energy in the ocean – solar, wind, and wave – are available only at the sea surface. Once an underwater vehicle descends below the ocean surface, it must carry onboard all of the energy supplies required to accomplish its objectives (one exception is discussed in Sect. 12.5).

The characteristic of being *autonomous* for any underwater vehicle also imparts certain benefits and limitations. The primary benefit of autonomy is providing the platform with the ability to accomplish useful objectives (collection of ocean measurements, cargo transport, military-relevant missions, etc.) without direct human input. This ability almost always results in large cost savings, and enables transits in areas too dangerous or inaccessible for humans. The major limitation, on the other hand, is associated with this lack of direct human input. Once it leaves the ocean surface, an autonomous underwater platform must have onboard all of the artificial intelligence required to accomplish its goals. Improving the level of onboard intelligence is the primary challenge to future applications in underwater robotics.

Given these attributes and limitations, UW gliders (and autonomous underwater gliders in particular) are capable of performing a variety of functions and missions. These functions can be categorized as follows [12.1].

12.3.1 Depth Unlimited Roaming

In depth unlimited roaming, the glider is not confined to a particular depth regime while transiting cross-country in a deep ocean environment. Often such roaming will require trans-basin round-trip excursions. The Seaglider and Spray are among this functional class, being designed primarily for the role of gathering ocean vertical profiles of water mass properties. Design adaptations for such depth unlimited roaming require some or all of the following capabilities: long range, cruise speeds adequate to penetrate large-scale ocean circulation but otherwise kept to a minimum to conserve onboard propulsion energy, small-to-moderate payload volume, minimized hotel loads, and deep dive capability with neutral hull compressibility.

12.3.2 Depth Limited Roaming

This function requires cross-country capability within a limited depth regime. This constraint arises when operations are required in the shallow water regimes of the littoral zone, or when the vehicle must operate in a prescribed sector of the water column such as a sound channel or avoid penetration across the thermocline. The Slocum has design adaptations for this role such as its piston pump that allows it to rapidly reverse dive direction in close proximity to the free surface or seabed in confined shallow water areas. Useful design adaptations for this role include: flat glide slope (high L/D) which simultaneously maximizes range for a minimum number of dive cycles, high sprint speed capability to penetrate strong coastal currents, small to moderate payload volume, minimized hotel loads, rapid high-resolution pitch and roll response to avoid broaching or grounding in confined depth regimes, adequate flight control authority for suppressing ocean-surface-wave induced flight oscillations, and avoidance measures for fishing trawlers.

12.3.3 2-D Station Keeping

Station keeping requires the ability to maintain position at a prescribed point in the ocean. Other than the case of free drifting in stagnation flow or grounding on the seabed, underwater gliders must execute depth excursions in order to maintain station at a fixed latitude and longitude. Hence, the station keeping ability is two-dimensional (2-D) and is referred to as 2-D station keeping. All three profiling gliders have demonstrated 2-D station keeping, some within a watch circle of several meters for several weeks at a time. Some station keeping roles may require the glider to profile the water column at a fixed latitude and longi-

tude, which might require maximum sprint and dive speed. Other station keeping roles may involve the glider maintaining station in a certain depth regime, which would benefit from the glider having minimum sink rate properties. In all cases, the glider needs adequate cruise speed to penetrate and hold station against ocean currents. In addition, the glider may be required to hold station on the seabed, in which case it must generate sufficient negative net buoyancy and/or have provisions in its hull and wing shape for anchoring against currents. Other vehicle qualities for station keeping would be long on-station capability, small to moderate payload volume, minimized hotel loads, rapid high-resolution pitch and roll response to execute grounding maneuvers or maneuvers near the seabed, adequate flight control authority when operating near the sea surface, and avoidance measures for fishing trawlers.

12.3.4 Payload/Cargo Delivery

The stealthy, high endurance (long distance combined with long duration) capabilities demonstrated by profiling gliders suggest that delivery of payloads and cargo would be logical function when rapid delivery time is not required. Among the most important characteristics for this breed of underwater glider would be the ability to move large payloads/cargo over significant horizontal distances while minimizing onboard energy consumption (i. e., using minimal numbers of dive cycles). Winged structures such can fly cooperatively to improve flight efficiency. Therefore, an UW glider can be equipped with cargo-carrying exterior compartments so that the total is *more* energy efficient in point-to-point transport than the glider alone, as discussed later in this chapter. This function may require both deep water and depth-limited operational capability (high L/D) with adequate cruise speeds to penetrate both large scale ocean circulation and coastal currents. In addition, large payload volume is required along with minimal hotel loads.

12.3.5 Level Flight Hybrids

This concept is posed to compensate for the major limitation of underwater gliders: the inability to maintain fixed depth in forward transit. This *motor-glider* is a glider with an auxiliary motor-driven screw. Prop-driven AUVs typically are ballasted for safety reasons to be slightly positively buoyant and use either vectored thrust or dive planes to achieve level flight. The motor-glider is a more efficient means for accomplishing the same force balance, using the lift from a high aspect ratio wing to provide the compensating trim

forces against buoyancy to maintain level flight. The concept is envisioned for circumstances where operations require short-term burst speed in very narrow depth regimes, or when level flight is required. Level flight capability may be required for proper operation of certain sensors like seafloor mapping sensors. High burst speed over a limited depth extent may be needed for certain avoidance maneuvers or for pene-

tration in strong shallow water currents. This hybrid propulsion system approach provides the basis for a long range, high endurance prop-driven AUV (autonomous underwater vehicle). Design adaptations for this role require many of the same characteristics as depth limited roaming, with the addition of low drag at high cruise speed to maximize prop-powered flight performance.

12.4 Optimal Size and Shape for Horizontal Transport Efficiency

Transport efficiency varies inversely with the cost of locomotion. It is commonly measured in transportation science by *specific energy consumption* or *net transport economy*, which is equal to the energy consumed per horizontal distance traveled for each unit of vehicle weight [12.7, 12]. Specific energy consumption differs from net transport economy in that the former is based only upon the energy expended in propulsion, whereas net transport economy includes all forms of vehicle energy expenditure including the hotel loads (energy consumed by control systems, communications, payload power requirements, onboard data processing, launch and recovery systems, etc.). Similarly, the vehicle weight can be defined in various ways, for example in terms of total dry bulk weight of the vehicle (including payload), $F_g = \bar{\rho}_s g V_s$. In the next part of this section, it is defined as the weight (net buoyancy force) $Mg = B$, due to the loaded mass M applied to a wing (Fig. 12.1). An alternative weight normalization for specific energy consumption considers only that of the payload/cargo, to eliminate any potential bias toward larger underwater vehicles.

12.4.1 Net Transport Economy

Analytic surveys of natural and man-made fliers provide a starting point for identification of present operating regimes of the profiling gliders and rules of scaling to other performance regimes from those gliders. Design surveys in aeronautical design and bio-mechanics has produced a number of useful works for this purpose [12.7, 12–15].

Analytic flight survey literature reveals that a leading order variable controlling regimes of scale is the loaded mass. In an underwater glider, the loaded mass is supplied by the buoyancy engine. The loaded mass (net buoyancy/g) can be used as the normalization factor in the *net transport economy* (NTE)

$$\text{NTE} = \frac{P}{(Bu)} = \frac{P}{(Mgu)}, \quad (12.5)$$

where P is the total time-averaged power consumed by the flier. The net transport economy is dimensionless and smaller values indicate more efficient transport. The dimensionless NTE is commonly compared to the loaded mass in kilograms [12.13]. Figure 12.8 plots NTE over 12 orders of magnitude variation in loaded mass, covering regimes of scale from insects to jet transports. The NTE values in Fig. 12.8 are based on total power consumption P including both the flight power spent overcoming drag ($P_e = DU$) as well as internal power consumption ($P - P_e$), which includes basal metabolic rates in the case of natural fliers and all subsystem energy consumption in the case of man-made fliers (hotel loads). In [12.13] and [12.15], estimates are made of the basal metabolic rates of birds based on the body mass, resulting in an empirical formulation of NTE

$$\text{NTE} = 0.898(Mg)^{-0.227} \quad (\text{Tucker Fliers}) . \quad (12.6)$$

References [12.12] and [12.14] also examined a limited set of data on birds and derived a similar empirical relation

$$\text{NTE} = 0.914(Mg)^{-0.293} \quad (\text{Schmidt-Nielsen Fliers}) . \quad (12.7)$$

These two empirical relations are indicated by the solid sloping lines in Fig. 12.8. The most apparent scale dependent feature of these empirical relations and the NTE data is that the energy consumed per meter traveled decreases as the loaded mass is increased – bigger fliers (greater loaded mass) are more efficient fliers. The profiling gliders presently operating in the range of 100–300 g of loaded mass are overlaid on Fig. 12.8 as a purple triangle. It appears that the profiling gliders are consuming relatively higher levels of energy per horizontal distance traveled than their bird/bat counterparts operating at equivalent loaded mass. Natural fliers are used as a standard for ultimate efficiency because natural selection tends to eliminate all but the most efficient mutations [12.13]. However, several factors

contribute to this apparent disparity in efficiency. First, the profiling gliders were not designed for efficiency in *horizontal* transport, but rather to move primarily up and down to collect vertical profiles of water column properties. For this case, then, a more useful form for (12.5) is to normalize by U , the speed along the glide slope, rather than the horizontal speed u . This change results in the net transport economy values from (12.5) being multiplied by $u/U = \cos(\gamma)$, where γ is the glide angle from the horizontal (Fig. 12.1). Since the profiling gliders are flown at glide angles of 20° to 30° , this factor results in only a 10% reduction in NTE. Second, rather than normalize the energy consumed per distance traveled by the weight of the loaded mass, NTE can be defined by normalizing by the dry bulk weight. Whereas this change in normalization usually has little effect on NTE for fliers in air (dry bulk weight usually is equal to the weight of the loaded mass), it causes a significant decrease in NTE for underwater platforms since the weight of the loaded mass can be remarkably different than the dry bulk weight due to the positive buoyancy of displaced water. Profiling gliders may be intrinsically less efficient relative to birds because of the extra energy that is consumed when gliding through ocean stratification, particularly when crossing the thermocline. Density changes in the ocean water mass cause corresponding changes in net buoyancy B , resulting in additional rate of working by gravity as defined by the right hand side of (12.1). A comparison of NTE for profiling gliders with (purple triangle) and without (yellow square) ocean stratification is provided in Fig. 12.8. Hull compressibility resulting from depth changes in the ocean cause additional changes in net buoyancy and in the work rates by gravity that ultimately factor against the total power consumption of the UW glider. No counterpart to this increment of energy consumption exists for birds flying in air. To minimize energy consumption due to hull compressibility, the optimal design solution is to match the hull compressibility with seawater compressibility. This match has been done on the deep-diving profiling gliders Seaglider and Spray that operate at very low values of loaded mass (net buoyancy), and where even small changes in net buoyancy can be critical to overall net transport economy.

For comparison, the NTE for the 6.2 m wingspan ZRay flying wing glider (presented later in Fig. 12.12), based on energy consumption measurements made at sea, is plotted in Fig. 12.12 as a red circle. Its NTE value of 0.65 is also somewhat above the Schmidt–Nielsen Fliers curve, but approaches it if the ZRay payload is removed (NTE drops to less than 0.45).

To further reveal relative differences in efficiency of the flying shapes, *specific energy consumption* (E_c) can be used. It is a transport economy formulation based

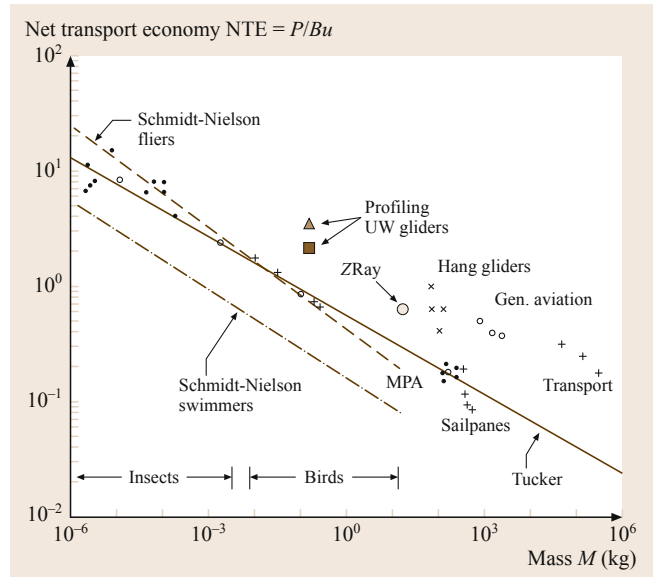


Fig. 12.8 Net Transport Economy (NTE) for natural and man-made fliers (after [12.12]) versus the profiling underwater gliders with (purple triangle) and without (yellow square) ocean stratification and the ZRay flying wing glider from at-sea measurements (red circle). NTE is based on total energy (propulsion plus hotel load and payload) consumption

only on the rate of expenditure of flight energy required to overcome drag ($P_e = DV = Bw$) ([12.7] and (12.1)). Energy is consumed by the buoyancy engine to generate a variable displaced volume increment $\pm V_b$, for forward propulsion. Only the horizontal component of the glide speed, u , results in horizontal distance traveled point-to-point. Consequently, the specific energy consumption (net transport economy) for horizontal transport of an underwater glider is

$$E_c = \frac{P_e}{\rho g V_b u} = \tan \gamma = \left(\frac{L}{D} \right)^{-1}. \quad (12.8)$$

The glide slope, $\tan \gamma$, is equal to the reciprocal of the lift-to-drag ratio $(L/D)^{-1}$, and provides a physical metric of horizontal point-to-point transport efficiency. In other words, specific energy consumption is minimized by achieving the flattest possible glide slopes. A flat glide slope allows an underwater glider to travel the greatest distance point-to-point for a given number of buoyancy engine cycles. A flat glide slope also enables shallow water operations and other kinds of depth limited applications. Using the conventional quadratic formulation in the β -plane for lift L , and drag D , forces normalized to the wing area A_0 [12.16]

$$L = \frac{1}{2} \rho C_L A_0 U^2 \quad \text{and} \quad D = \frac{1}{2} \rho C_D A_0 U^2. \quad (12.9)$$

Here, C_L and C_D are the quadratic lift and drag coefficients, respectively. The drag coefficient is made up of two terms, a profile drag term C_{D0} , that depends on Reynolds number R_e , and an induced drag term C_{Di} , that increases with increasing lift coefficient and decreases with wing aspect ratio, N_R [12.17]

$$C_D = C_{D0} + C_{Di} = K_0 R_e^{-\xi} N_A + K_i \frac{C_L^2}{\pi N_R}. \quad (12.10)$$

In (12.10), K_0 is the profile shape factor, N_A is the ratio of the total wetted surface area to the wing area $N_A = A_t/A_0$, and K_i is the wing plan form factor. The aspect ratio is defined as $N_R = S/\bar{c} = S^2/A_0$ where S is the wingspan and $\bar{c} = A_0/S$ is the mean aerodynamic chord of the glider's wing. The power-law dependence of profile drag is $\xi = 1/2$ for completely laminar, un-separated boundary layer flow over the vehicle, and $\xi = 1/5$ for fully turbulent un-separated boundary layers. In (12.10), the Reynolds number is the size-dependent scale factor $R_e \equiv U\bar{c}/\nu$, where ν is the kinematic viscosity of the fluid. Since the glider is considered a streamlined body, the Reynolds number dependence of the profile drag term in (12.10) is an approximation of friction acting on the total wetted area, A_t . Specific energy consumption, E_c , can be explicitly examined for efficient gliders that achieve small glide angle during coordinated wings-level flight ($v = v' = 0$; $\beta = 0$). With the small glide angle assumption, the lift-to-drag ratio can be written after [12.18] as

$$\frac{L}{D} = \frac{C_L}{C_D} = \frac{u^2}{K_3 u^4 + K_4} = \frac{1}{E_c}, \quad (12.11)$$

where

$$K_3 = \frac{A_0}{2gV_b} K_0 R_e^{-\xi} N_A, \\ K_4 = \frac{2gV_b}{A_0} \frac{K_i}{\pi N_R}.$$

Taking $\partial(L/D)/\partial u = 0$, the speed at which the lift-to-drag ratio is maximized becomes $U = (K_4/K_3)^{1/4}$ giving

$$\left(\frac{L}{D}\right)_{\max} = \frac{1}{2} (K_3 K_4)^{-1/2} = \frac{1}{(E_c)_{\min}}. \quad (12.12)$$

It can be readily shown that the small glide angle approximation ($L \approx B = \rho g V_b$) also reduces the Reynolds number to

$$R_e \equiv \frac{U\bar{c}}{\nu} \cong \frac{1}{\nu} \left(\frac{2gV_b}{C_L N_R} \right)^{1/2}.$$

Using this approximation to eliminate the Reynolds number in (12.10) and (12.11) gives the minimum specific energy consumption for nonturning, steady-state

flight in (12.12) as [12.18]

$$(E_c)_{\min} = 2 \left[\frac{\nu^\xi K_i K_0 C_L^{\xi/2} N_A}{\pi (2gV_b)^{\xi/2} N_R^{1-\xi/2}} \right]^{1/2} \\ = \left(\frac{L}{D} \right)_{\max}^{-1}. \quad (12.13)$$

12.4.2 Size Factors

The minimum specific energy consumption from (12.13) decreases as $V_b^{-\xi/4}$, i. e., it decreases with increasing net buoyancy. Because net buoyancy is some fraction n_b of the total vehicle volume V_0 , where $V_b = n_b V_0$, bigger buoyancy-driven vehicles generally are more transport efficient. Actually, surveys of natural and man-made fliers by [12.12] and [12.14] demonstrate that specific energy consumption monotonically decreases across 12 orders of magnitude of size increase. This size advantage is accentuated in an underwater glider because the buoyancy volume factor, n_b , increases with increasing vehicle volume approximately as $n_b \approx 1.2 \times 10^{-5} V_0^{7/6}$, due to economies of scale in packing efficiency [12.7]. Larger n_b permits higher glide speeds (speed increases as the square root of the increase in net buoyancy) and higher wing section Reynolds numbers, which results in higher wing section lift-to-drag ratios (Fig. 12.9).

Equation (12.13) also indicates that specific energy consumption decreases with increasing aspect ratio of the wing, as $N_R^{-(1-\xi/2)/2}$, favoring long tapered wingspans with relatively small wing chords. The aspect ratio of the profiling gliders varies from a maximum of $N_R = 9.75$ for Spray to a minimum of 4.4 for Seaglider. Specific energy consumption decreases as the lift to drag ratio (L/D) increases, but L/D suffers a precipitous decline if the wing section chord is made too small in an effort to achieve a high aspect ratio. Figure 12.9 shows that this L/D crisis occurs when the wing section Reynolds number drops into the mid 10^4 regime. This phenomenon arises because of laminar separation on the suction side of the wing section, which destroys a large percentage of the lift. Profiling gliders with their present 10–20 cm wing chords and 30 cm/s cruise speeds are operating within the laminar separation regime where their wings will not be able to realize a higher L/D and lower E_c by simply flying at higher angles of attack (Fig. 12.9). This laminar separation phenomenon suggests a need to go to bigger wing chords to get above the mid 10^4 Reynolds number regime in order to improve flight efficiency. A primary design philosophy of the larger cross-country gliders (Fig. 12.4) is to achieve

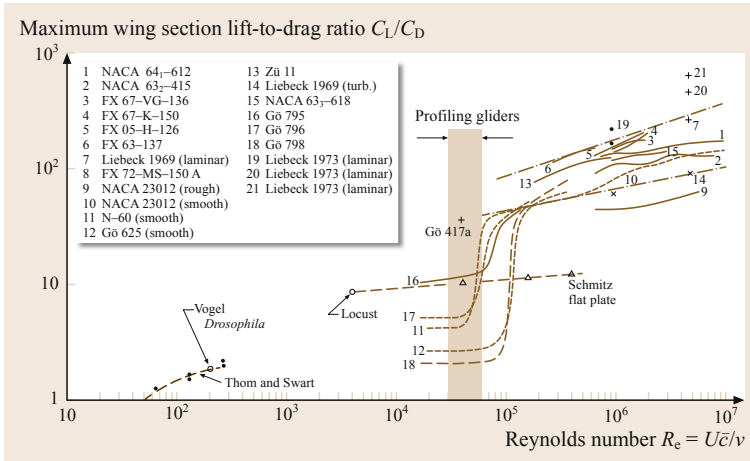


Fig. 12.9 Variation in maximum airfoil section lift-to-drag ratio with Reynolds number (after [12.12]). Numbered curves according to airfoil sections in the inset table

sufficiently large wing chords to avoid the L/D crisis shown in Fig. 12.9. Since Fig. 12.10 indicates that the wing area of profiling gliders is properly sized, larger wing section chords would reduce the wing aspect ratio ($N_R = A_0/\bar{c}^2$).

Increases in wing aspect ratio to reduce specific energy consumption are not only constrained by Reynolds number effects, but by material strength properties as well. As wing aspect ratio increases for a given wing area, the mean wing chord and so the Reynolds number of the wing section decreases, causing degradation of the maximum lift-to-drag ratio of the wing section according to wind tunnel measurements [12.19–21]. If the aspect ratio is increased by increasing the span, the weight of the wing, F_W , will increase as $F_W \approx S^{5/3}$. As the wing weight increases, the thickness-to-chord ratio of the wing section, \bar{t}/\bar{c} , must be increased as $\bar{t}/\bar{c} \approx S^{1/6} \approx V_0^{1/9}$ to provide adequate span-wise bending strength and torsional stiffness [12.22]. If \bar{t}/\bar{c} is made excessively large to satisfy strength requirements of a high aspect ratio wing, then the maximum lift-to-drag ratio of the wing section will further degrade [12.19, 20] and [12.21]. For natural fliers, wing dimensions scale with total volume as $S \approx V_0^{1/3}$ and wing area as $A_0 \approx 0.165V_0^{2/3}$ according to the *square-cubed law* originally proposed by Cayley, and critiqued later in [12.12]. Based on dimensional analysis, the basic square-cubed law specifies

- Wing semispan: $b \sim M^{1/3}$,
 - Wing area: $A_0 \sim 0.165M^{2/3}$,
- (12.14)

where M again is the loaded mass.

Figure 12.10 suggests that nature has found a compromise between transport efficiency and structural limitations at an aspect ratio of about $N_R = S^2/A_0 = 6.1$. Inspection of Fig. 12.10a indicates the wing semispan of

the profiling gliders may be a bit excessive for the loaded mass at which they operate, but that the wing area of the profiling gliders in Fig. 12.10b compares closely with nature, fitting almost exactly the square-cube law formulation in (12.14), refined by Tucker (contained and discussed in [12.12]) from measurements of birds. Hence, the lack of comparable efficiency of the shapes of the profiling gliders appears not to be due to insufficient wing area, but rather because the loaded mass M is too small or the wetted surface area A_t is too big, or both. From analysis of observational measurements of birds in wind tunnels and in natural environments, Tucker has extracted an empirical relation for specific energy consumption of natural fliers [12.12]

$$E_c = 0.109(Mg)^{-0.185}. \quad (12.15)$$

Note that the exponent in this expression does not differ significantly from that in the empirical fit to NTE in (12.6); they only differ in the size of the leading exponent. From this empirical formulation, it appears that profiling gliders are less efficient fliers in horizontal transport (larger E_c when normalizing by loaded mass) than Tucker's equation would predict. Hence, it appears that horizontal transport efficiency can be further improved in profiling UW gliders (they were designed to profile vertically, not optimize horizontal transport efficiency). This improvement in E_c was a primary guiding factor in developing the larger underwater gliders shown in Fig. 12.4.

12.4.3 Shape Factors

Of all the geometric properties of the glider, the wetted surface to wing area ratio $N_A = A_t/A_0$, has the strongest influence on the specific energy consumption, increasing as $N_A^{1/2}$ (12.13). This result suggests that design focus on reducing N_A will achieve the greatest improvements

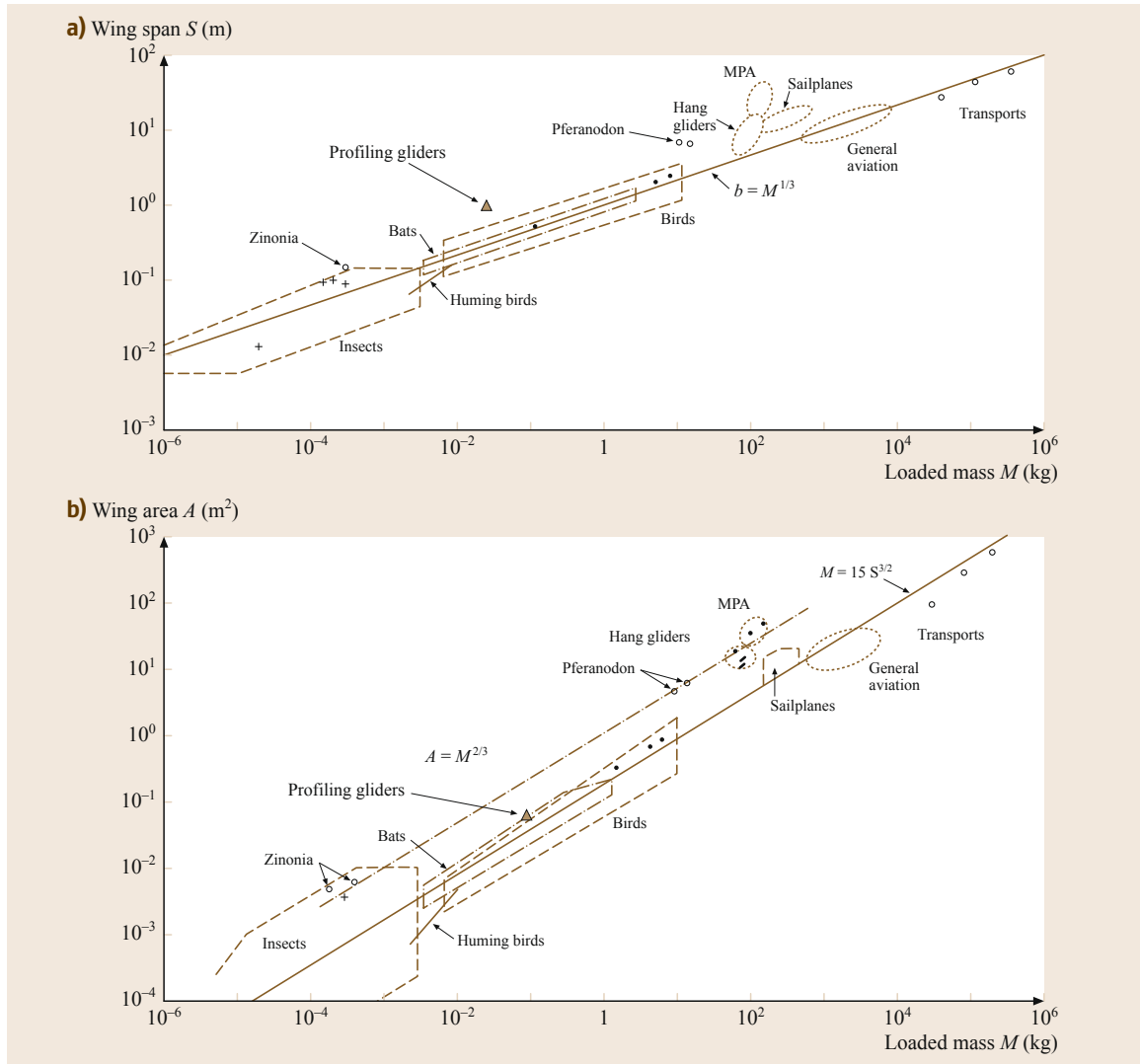


Fig. 12.10a,b Characteristic wing dimensions as a function of loaded mass. **(a)** Scaling of wingspan as a function of loaded mass; **(b)** wing area as a function of loaded mass for natural and man-made fliers (after [12.12, 18])

in horizontal transport economy. As a benchmark in underwater gliders, *Seaglider* has an $N_A = 21.1$ [12.3]. However, the smallest N_A values are associated with *flying wing* and *blended wing/body* geometries, such as utilized by birds, for which typically $N_A \approx 2.2$ to 2.4. The other benefit derived from concentrating the vehicle volume in the wing itself is a large wing area that reduces the magnitudes of C_L and the associated induced drag (the largest component of the drag at minimum E_c). Equation (12.13) indicates that specific energy consumption grows as $C_L^{\xi/4}$. However, increasing wing area indefinitely to achieve a low C_L becomes mutually exclusive with high aspect ratio, N_R . In (12.13), the factor $C_L^{\xi/2} / N_R^{1-\xi/2}$ indicates that a large N_R exerts a greater

reduction in E_c than does a proportionally smaller C_L , subject to the structural limits mentioned above.

Another issue with concentrating vehicle volume in the wing is the effect on the profile drag shape factor K_0 . Shape efficiency comparisons based on K_0 between a 2-D flying wing and a three-dimensional (3-D) winged body of revolution should be based on the same vehicle volume, V_0 . Considering both shapes are streamlined bodies, K_0 scales in proportion to the wetted surface area relative to volume as $A_t / V_0^{2/3}$. Taking an ellipse as the canonical cross section for both 2-D and 3-D shapes, and following the assumption taken in [12.23] and [12.24] that the skin friction per unit area is the same for each shape, the shape factor ratio at con-

stant volume becomes

$$\frac{K_0(2\text{-D})}{K_0(3\text{-D})} = \frac{\pi A_t(2\text{-D})}{4 A_t(3\text{-D})} \approx \pi \sqrt{\frac{2(1-e^2)}{2-e^2}}, \quad (12.16)$$

where $e(0 \leq e \leq 1)$ is the eccentricity of the ellipse taken here as a proxy for the length-to-thickness ratio (*fineness*) of the body. Equation (12.16) is consistent with empirical data on drag of streamlined shapes at high Reynolds numbers (turbulent flow regime) [12.22]. These empirical data relatively show higher profile drag for 2-D shapes at small fineness ratios, as is the case in (12.10) when $e \rightarrow 0$. The data for 3-D shapes develop relatively higher profile drag at large fineness ratios, as occurs with (12.16) when $e \rightarrow 0.99$. Both the empirical data and (12.16) indicate a 2-D flying wing may suffer as much as a 3-fold increase in K_0 relative to a 3-D body of revolution. However, that increase is more than offset in (12.13) by a 9-fold reduction in N_A when a flying wing is compared to a winged body of revolution. For comparison, Fig. 12.11 shows a computational fluid dynamical (CFD) simulation of the Liberdade/XRay flying wing glider with vehicle volume of $V_0 = 1000$ L versus a Seaglider scaled up to a comparable size of $V_0 = 1000$ L. The winged body of revolution in the 1000 L class of glider has about a 30% advantage in maximum cross country speed over the flying wing, but the flying wing is about 43% more efficient in horizontal transport.

Comparative analyses of transport economy in large subsonic transport aircraft concur with this conclusion, generally finding a 20–25% advantage in lift-to-drag ratio for the flying wing over conventional winged bodies of revolution, with additional benefits in gross take-off weight, operating weight per passenger, and fuel consumption per passenger [12.25]. Other factors not immediately apparent in (12.13) that favor the 2-D flying wing geometries for underwater gliders are: higher Reynolds number on the wing section (due to larger wing chord), leading to higher maximum lift-to-drag ratios (thereby avoiding the 10^4 Reynolds number regime in Fig. 12.9) [12.12]; and increased structural depth of the center section allowing increases in wingspan (and aspect ratio) with fewer weight penalties compared to winged bodies of revolution [12.25, 26].

Together, (12.13) through (12.16) indicate four distinct adjustments that can be made to vehicle characteristics to get energetically more efficient in horizontal transport than the profiling gliders:

1. Increase the buoyancy engine volume to the maximum extent possible for the given internal volume
2. Make the underwater gliders bigger
3. Reduce the total vehicle wetted area A_t relative to the wing area, and

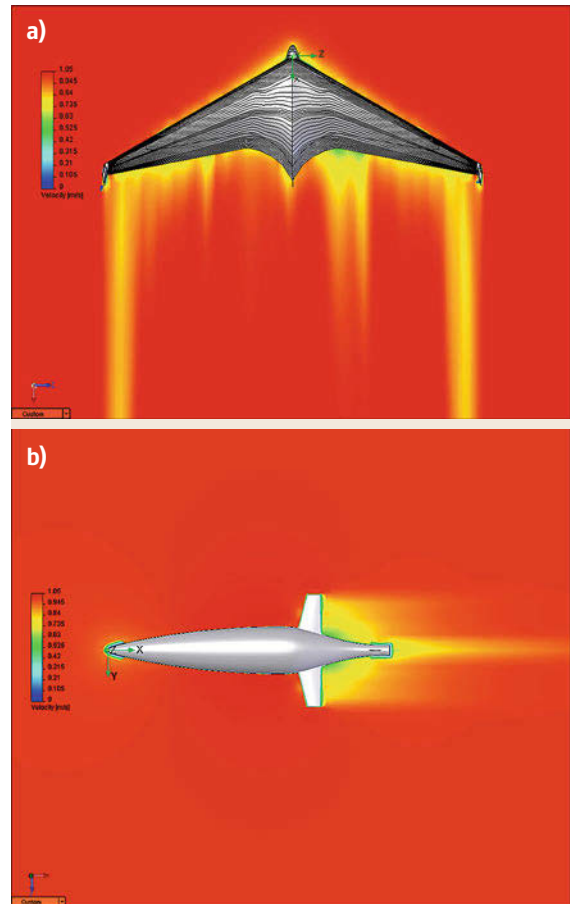


Fig. 12.11a,b Computational fluid dynamical (CFD) simulation of velocity field (using after [12.27]) in the horizontal plane for (a) Liberdade/XRay at $(L/D)_{\max} = 19$, and (b) profiling-type Seaglider scaled up to $V_0 = 1000$ L at $(L/D)_{\max} = 11$. The surface roughness is $10 \mu\text{m}$ in both simulations

4. Increase the wing aspect ratios to the maximum extent possible without reducing wing chord to such a degree that it operates in the mid 10^4 Reynolds number regime.

The wetted area could be reduced by copying birds and designing underwater gliders with flying wing or blended wing body shapes (Fig. 12.12). However, the form factors of such shapes have lower packing efficiency for the glider subsystems that typically fit more readily into cylindrical or spherical shapes.

12.4.4 Glide Polar

Glider flight efficiency is not only just a function of vehicle characteristics, but also a function of how the

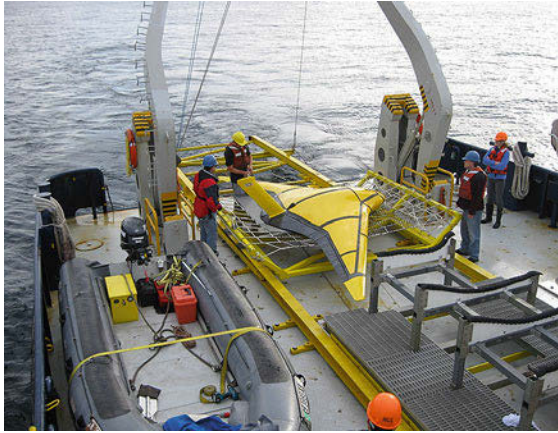


Fig. 12.12 Liberdade/ZRay blended wing body glider aboard R/V Sprout, January, 2011

glider is flown. The expression for specific energy consumption in (12.13) shows that flight energy consumption is minimized by maximizing the lift-to-drag ratio, L/D . From the proportionality between the force and speed triangles in Fig. 12.1, a relation exists between the maximum L/D achievable for a given glider and the angle of the glide path. Since the profiling gliders are flown at glide path angles between 20° and 30° in order to profile the ocean temperature and salinity fields, they will not achieve a specific energy consumption any better than $E_e \approx 0.3$ to 0.5 no matter how optimal their physical characteristics are made. In most ocean environments, the horizontal scales of variability are sufficiently large that vertical profiles of the water column can be collected at significantly shallower glide slopes. So the gliders in the functional class of *depth unlimited roaming* would benefit from improved horizontal flight efficiency, assuming their existing desirable characteristics (e.g., two-person portability) can be retained. However, in other functional classes, maximum flight efficiency in the horizontal is much more important. In particular, *depth limited roaming* requires a glider to travel long distances in a restricted depth interval, *payload/cargo delivery* vehicles must transport large payload and cargo over long distances point-to-point, and *level flight hybrids* must fly at a very flat glide path angle to minimize the expenditure of energy on auxiliary propulsion. All these types of applications for UW require minimum NTE and E_e , and hence maximum L/D . The specific energy consumption for the ZRay flying wing glider demonstrated at sea is 0.05 and the NTE less than 0.65 .

While the L/D varies with glide path angle, a corresponding change occurs in the proportions of the speed triangle in Fig. 12.1. This proportional change in the speed triangle with changing glide slope angle yields

a continuous relationship between the horizontal and vertical components (w versus u) of the glide velocity, U . This relation, known as the *glide polar*, is readily derivable by balancing the forces in the vertical and horizontal for steady-state flight. Based on the quadratic formulation of lift and drag in (12.9) and (12.10), it is given by

$$w = \pm \left(\frac{\rho g V_b \sqrt{1 + \tan^2 \beta_z}}{(1/2) \rho A_0 (1 + H^2(\alpha)) \sqrt{C_L^2(\alpha) + C_D^2(\alpha)}} \right)^{1/2}, \quad (12.17)$$

where the polynomial H is a function of angle of attack α

$$H(\alpha) \equiv \frac{L}{D} = \frac{C_L(\alpha)}{C_{D0}(\alpha) + C_{Di}(\alpha)}, \quad (12.18)$$

and β_z is the bank angle from [12.28] given as,

$$\beta_z = \arcsin[\cos \varphi \sin \beta \cos \eta + (\cos \alpha \sin \varphi - \sin \alpha \cos \varphi \cos \beta) \sin \eta]. \quad (12.19)$$

In (12.19), φ is the pitch angle, β is the roll angle, and η is the yaw angle. In coordinated flight, $\eta = 0$, the bank angle approaches the angle of roll at small pitch angles, i.e., $\beta_z \rightarrow \beta$ as $\varphi \rightarrow 0$. Positive values of w in (12.17) correspond to ascending glides and $w < 0$ corresponds to descending glides. The corresponding expression for u is the same as (12.17) except that (a) only positive values of the horizontal speed are considered (the glider does not fly backward) and (b) $H^2(\alpha)$ changes to $H^{-2}(\alpha)$. The glide polars of the XRay flying wing glider (Fig. 12.11a) are plotted as solid lines in Fig. 12.13 for noncircling, wings-level flight at four different wing loadings within a potential range of net buoyancy volume, $n_b = V_b/V_0 = 3.8$ to 27.6% . The four polars in Fig. 12.13 (red, black, green, and blue curves) are representative of various buoyancy engine technologies, where the red curve ($V_b = 38.36$ L, $n_b = 3.8\%$) is representative of the upper end of the closed-loop liquid-based engine technology [12.2, 3], the black curve ($V_b = 50.0$ L, $n_b = 5.0\%$) represents the upper range open-loop liquid-based engine technology [12.1, 4, 29], the green curve ($V_b = 122$ L, $n_b = 12.2\%$) is a proxy for the open-loop compressed gas-based systems [12.8], and the blue curve ($V_b = 275$ L, $n_b = 27.6\%$) approximates the upper end of the open-loop gas-based buoyancy engines that consume gas generating compounds [12.5]. The magnitude of the glide velocity, U , and the velocity components (u , v , w) increase as the square root of the buoyancy engine volume increase and the associated wing loading (ratio

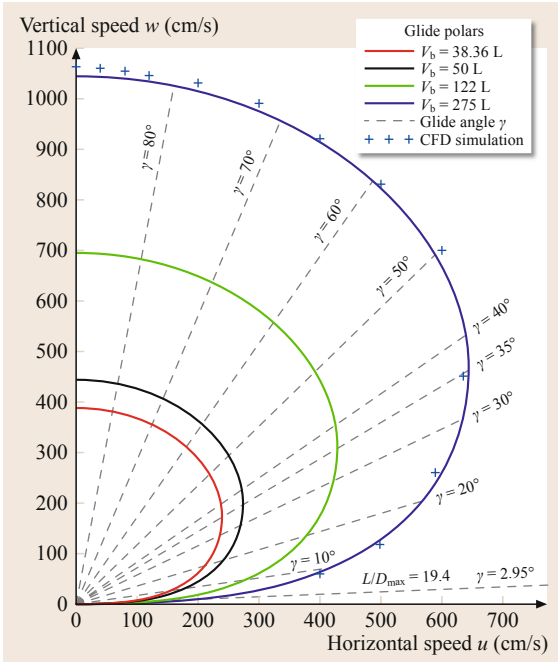


Fig. 12.13 Liberdade/XRay glide polars in the z -plane for wings level ($\beta = 0^\circ$) attitude over a range of net buoyancy between 38.36 and 275 L. Glide angles γ shown as *dashed gray lines* are invariant with net buoyancy change. *Blue crosses* are derived from CFD simulations at $V_b = 275$ L using (after [12.27]). See also Fig. 12.11a

of net buoyancy to wing area) [12.28, 30]. The maximum lift-to-drag ratio over ground (minimum specific energy consumption) is given by the point of tangency on the glide polar to a straight line drawn from the origin [12.28, 30]. The dashed gray tangent line in Fig. 12.13 indicates XRay has a predicted $(L/D)_{\max} = 19.4$, which corresponds to a best glide angle $\gamma = 2.95^\circ$ and a specific energy consumption of $E_e = 0.051$. With $10\ \mu\text{m}$ surface roughness, the CFD simulations like those in Fig. 12.11a gave approximately the same results, $(L/D)_{\max} = 20.0$. At-sea results for ZRay without the use of trailing edge flaps to change camber confirm these maximum lift-to-drag ratio results.

For comparison, the published polar of the Seaglider [12.3] gives a $(L/D)_{\max} = 7.0$, or $E_e = 0.143$. If the Seaglider with net buoyancy of $V_b = 0.33$ L was scaled up from its present volume of $V_0 = 66$ L to an equivalent volume of XRay of $V_0 = 1000$ L and given a net buoyancy $V_b = 38.36$ L, (Fig. 12.11b), then by (12.17), the maximum lift-to-drag ratio would increase by a factor of 1.81. This increase is based on the assumption of all laminar boundary layers ($\xi = 1/2$) in (12.17) and would give the scaled-up Seaglider a $(L/D)_{\max} = 12.7$. For all turbulent boundary lay-

ers ($\xi = 1/5$), (12.11) gives a $(L/D)_{\max} = 8.9$ for the scaled-up Seaglider. A CFD simulation (using [12.27]) for the scaled-up Seaglider (Fig. 12.11b) finds that about 60.5% of the boundary layer is laminar for a surface roughness of $10\ \mu\text{m}$, giving a $(L/D)_{\max} = 11.1$.

When the XRay glider is flown at steeper glide angles (shown by the other dashed gray radial lines in Fig. 12.13 above the tangent line of the best glide angle $\gamma = 2.95^\circ$), the cross-country speed, u , increases, reaching a maximum at a glide angle $\gamma = 35^\circ$. This maximum arises because C_D is nearly invariant with C_L , when C_L becomes small at the small angles of attack during steep glides. In this case, an equation for u analogous to (12.17) reduces to u being dependent on $\sin \gamma \cos^2 \gamma$, where $\gamma = \arctan(H^{-1})$. This expression has a maximum at $\gamma = 35^\circ$ [12.1]. Within its range of possible buoyancy variation, the maximum country speeds of XRay can theoretically vary over a wide range, from $u_{\max} = 241$ cm/s (4.7 kts) at a net buoyancy of $V_b = 38.36$ L (red curve), reaching $u_{\max} = 644$ cm/s (12.5 kts) at a vehicle net buoyancy of $V_b = 275$ L (blue curve). XRay's glide speeds along the $\gamma = 35^\circ$ glide slope, referred to as \hat{U} , are found in Fig. 12.13 to be $\hat{U} = 296$ cm/s (5.8 kts) at a net buoyancy $V_b = 38.36$ L, reaching $\hat{U} = 793$ cm/s (15.4 kts) at the maximum vehicle net buoyancy of $V_b = 275$ L. These numerical results, confirmed by at-sea tests, indicate that the XRay flying wing glider fitted with moderately sized buoyancy engines (the as-built XRay glider has $V_b = 30$ L) is capable of traveling point-to-point at horizontal speeds comparable to those of commercially available, mid-size prop-driven autonomous underwater vehicles (AUVs).

The glide polars for Seaglider [12.3] give $u_{\max} = 46$ cm/s (0.89 kts) at a net buoyancy $V_b = 0.33$ L, ($n_b = 0.5\%$). For the scaled-up Seaglider at $V_0 = 1000$ L and $V_b = 38.36$ L, the wing loading is increased by a factor of 47, thereby increasing cross-country speed to $u_{\max} = 315$ cm/s (6.1 kts) based on application of the wing loading relationship expressed in (12.17) to the published polar. As stated earlier, the winged body of revolution in the 1000 L class of glider has about a 30% advantage in maximum cross-country speed over the flying wing, although the flying wing is about 43% more efficient in horizontal transport.

Maximum along-coarse speed in still water is always obtained at a 35° glide angle regardless of vehicle shape or other hydrodynamic properties [12.1]. Figure 12.14 compares the potential cross-country speeds as a function of loaded mass (mass equivalent net buoyancy) of the four classes of underwater gliders when optimally sized for their intended missions. These include the winged body of revolution carrying single (small) payloads (*red*), the winged body of revolution carrying variable (large) payloads (*blue*), the flying

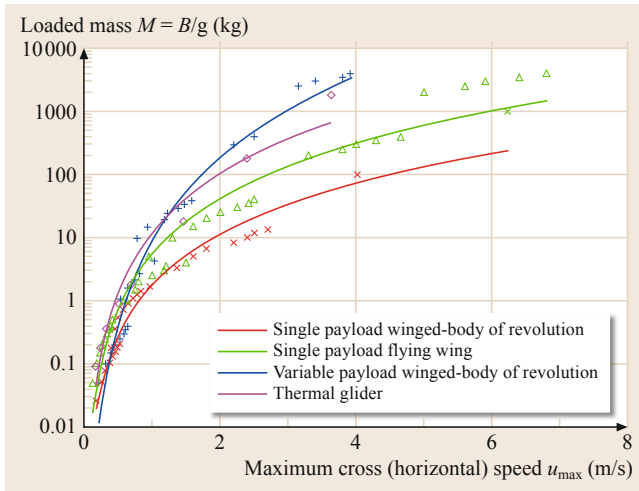


Fig. 12.14 Maximum cross-country (horizontal) speed for an underwater glider due to variation in the loaded mass for a winged body of revolution carrying single (small) payloads (*red*), a winged body of revolution carrying variable (large) payloads (*blue*), the flying wing carrying single (small) payloads (*green*), and a thermal glider in a winged-body-of-revolution configuration with single payload (*purple*)

wing carrying single (small) payloads (*green*), and the thermal glider in a winged-body-of-revolution configuration with single payload (*purple*). Winged bodies of revolution with maximum buoyancy engine capacity are the optimal combination for maximum speed (Fig. 12.15). For a given n_b , flying wings of equivalent vehicle volume are slower than winged bodies of revolution, but have superior transport economy, requiring fewer dive cycles (and less near surface exposure time) for a given distance traveled.

To exploit the superior horizontal transport economy of the flying wing for large payloads and cargo, vehicle packing must deal with the planar form factor of the flying wing and distribute the vehicle weight such that the critical vehicle balance factors that provide stability are met both before and after payload/cargo delivery. Those critical balance factors are (1) adequate vertical separation between the centers of buoyancy and mass, and (2) adequate horizontal separation between the centers of pressure and mass. A large payload/cargo concept for the flying wing glider is based on the use of multiple wing systems, and is referred to as the *Coanda triplane*, Fig. 12.16. The concept is based on adding two auxiliary wings to the basic ZRay flying wing glider hull form. To assure maximum vertical separation between the centers of buoyancy and mass, the lower wing carries the negatively buoyant payload/cargo while the upper wing carries buoyancy-compensating foam. This arrangement allows the glider to deliver the payload/cargo

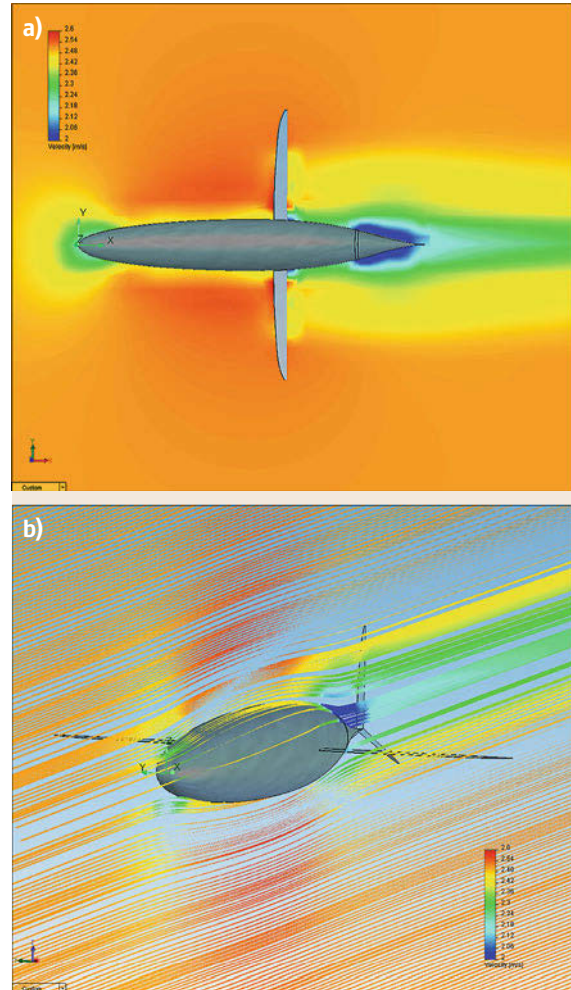


Fig. 12.15a,b CFD simulations of *The Bus* concept, a large winged body of revolution for carrying large payloads, used for creating the blue curve in Fig. 12.14. (a) Velocity contour plot in the horizontal plane; (b) streamlines in the vertical plane of *The Bus*

to the seafloor without having to perform unusual flight behaviors; upon arrival at the deployment site, the upper and lower wings are released, transforming the vehicle into a conventional ZRay glider.

The upper and lower external wings have high thickness-to-chord cambered airfoil sections. Computational fluid dynamical simulations (Fig. 12.17) show that for a particular-sized separation between these cambered auxiliary wings and the symmetric ZRay main-body wing section, remarkably high lift coefficients (large aggregate flow circulation) can be obtained at low angles of attack during both descent and ascent. This phenomenon is attributable to the *Coanda effect*, whereby the high velocity flow through the two gaps

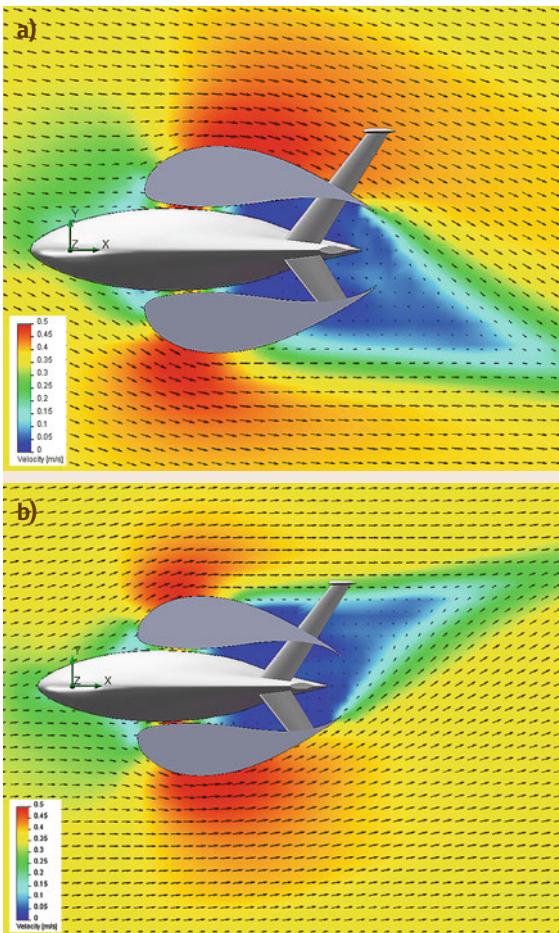
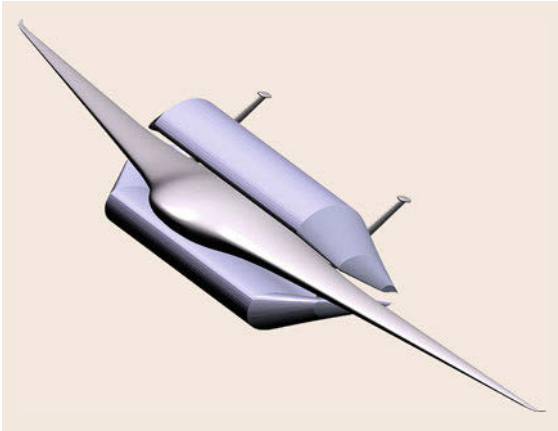


Fig. 12.17a,b A CFD study of the wing circulation for the Coanda triplane. (a) Shows the velocity contours during descending dives at negative angles of attack while (b) shows the velocity contours during ascending dives at positive angles of attack

Fig. 12.16 The Coanda triplane is a large flying wing glider based on the ZRay glider (Figs. 12.4b and 12.12) for carrying large payloads and cargo to be delivered on the seafloor. The lower wing carries the negatively buoyant payload/cargo while the upper wing carries the foam for buoyancy compensation ◀

between the three wing sections remains attached in the diverging flow over the aft surfaces. This phenomenon results in a high degree of flow circulation in a closed-ended wake behind the aggregate three-wing system. The circulation is clearly visible by the vertical asymmetry of the velocity contour plots in Fig. 12.17 and by the progressive vector arrows. The lift coefficient that results from this circulation is on the order of $C_L = 2.8$, and translates into a near doubling of the L/D over that of ZRay alone. The glide polar for the Coanda triplane concept, computed from CFD simulations, is plotted as the dashed black curve in Fig. 12.18. A maximum L/D of 37.7 is achieved, equivalent to a ZRay glider using 10° of camber-changing, trailing-edge flaps. However, the triplane is about 10 cm/s to 20 cm/s slower than ZRay, and achieves its best L/D at a glide speed of only

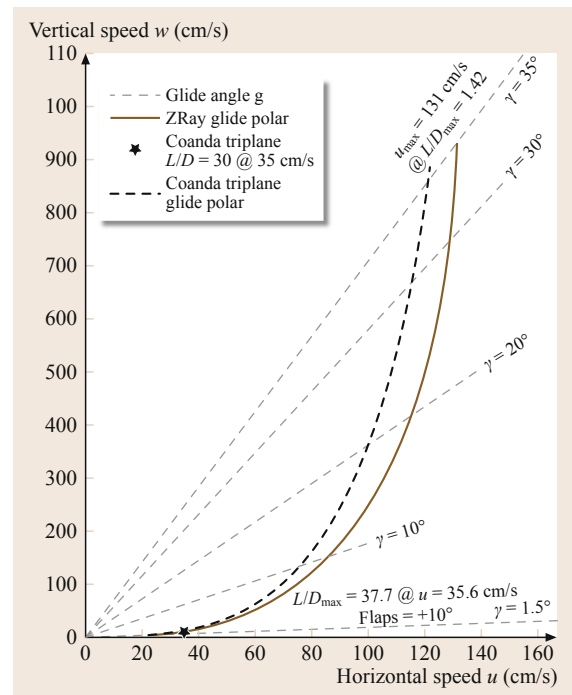


Fig. 12.18 Low-speed portion of the glide polar of the Coanda triplane concept (dashed black curve) and the ZRay glide polar (red curve). The glide polars are for wings level ($\beta = 0^\circ$) attitude for a net buoyancy of 13.15 L. Glide angles γ are shown as dashed gray lines

35.6 cm/s. The low speed characteristics at maximum L/D are largely a consequence of the triplane's relatively high wetted surface area.

In summary, the ZRay glider becomes *more* energy efficient in horizontal transport of large cargo and payload than when flying by itself, although it does so at

slower speeds. More generally, vehicles with wings can reduce their propulsion energy consumption by flying cooperatively with other wings, in contrast to prop-driven vehicles. Cooperative flight is enabled by the simplicity of the wing's trailing edge vortex system – Sect. 12.2.

12.5 Thermal Glider

This vehicle is applicable for ultra-long range, depth-unlimited roaming and for high endurance station keeping [12.4] (Table 12.1). The concept gives the glider the ability of renewing its onboard energy stores by harvesting environmental energy from the heat reservoir of the ocean, specifically from the temperature differences of the cold deep water and the warmer surface water (available in 80% of the world's oceans). Ranges of 30 000 to 40 000 km, circumnavigating the world, then become conceivable. Harvesting this thermal energy depends on the volume change associated with the state (phase) change of a material with a melting/freezing point in the range of ocean temperatures. Heat is absorbed from the warm surface water, causing a change of state from solid to fluid (melting), and released to the cooler, deeper water during the vehicle's transit through the thermocline, resulting in a state change back to the solid state (freezing). The heat exchange volume occurs inside tubes that run the vehicle's length and provide a large surface area for rapid heat flow. Almost all materials have a positive thermal expansion coefficient so that melting causes an increase in volume and freezing results in a decrease in volume (water below 4 °C is an exception). Because these volume changes are opposite to those required of a glider's buoyancy engine, they cannot be used directly for forward propulsion. Rather, the thermal buoyancy engine must include unique design features to account for the positive thermal expansion coefficient (as in Fig. 12.19) or the energy from expansion/contraction must be stored onboard over a half

dive cycle to be useable for propulsion. The four stages of the thermodynamic cycle are shown Fig. 12.19. Environmental energy is harvested by heat flowing into and out of the working fluid in chamber 1, which contracts on freezing and expands on melting. The resulting work is transmitted around the system by the transfer fluid, typically mineral oil. Chamber 2 is an energy storage accumulator, with the transfer fluid pressurized by nitrogen at a pressure greater than the maximum external ocean pressure. In Fig. 12.19a, the vehicle is in stable thermal equilibrium in the warm surface water, N₂ is compressed, the external bladder is inflated, and working fluid is expanded. Descent begins by opening the three-way valve (Fig. 12.19b), venting the external bladder to the internal bladder. Maintaining the hull interior slightly below atmospheric pressure creates the pressure differential for this flow. As the vehicle reaches cold water, heat flows out of the working fluid, which freezes and contracts, and draws in mineral oil from the internal reservoir. The beginning of ascent (Fig. 12.19c) results from opening the three-way valve, the pressurized oil in the accumulator moves to the external bladder and the vehicle changes from negative buoyancy to positive buoyancy. During ascent (Fig. 12.19d), the vehicle ascends to warm waters, heat flows into the working fluid, which melts and expands, and oil flows to recharge the accumulator.

Because the thermal glider is nearly identical in shape and dimensions to the winged body of revolution for single payloads, the glide polar data from Fig. 12.14 can be used for hydrodynamic input to an analysis of

Table 12.1 Analysis results for the net transport economy of various sizes of a thermal glider designed for the ultra-long range, depth-unlimited roaming application (after [12.1])

Scale [L]	Vol. [L]	Net buoyancy [L]	u	w [m/s]	Range [km]	NTE	Re vol ^(1/3)	Cd vol ^(2/3)
0.5	62	0.09	0.17	0.11	35 000	0.61	3.2×10^4	0.062
1	64	0.18	0.24	0.16	35 000	0.22	4.6×10^4	0.062
2	67	0.36	0.33	0.22	35 000	0.08	6.6×10^4	0.062
5	76	0.9	0.51	0.33	35 000	0.02	1.1×10^5	0.06
10	91	1.8	0.69	0.45	35 000	7.5×10^{-3}	1.7×10^5	0.059
100	358	18	1.46	0.95	35 000	3.6×10^{-4}	8.8×10^5	0.049
1000	3036	180	2.39	1.55	35 000	2.2×10^{-5}	5.9×10^6	0.036
10 000	29 809	1.80×10^3	3.63	2.36	35 000	1.4×10^{-6}	4.2×10^7	0.032

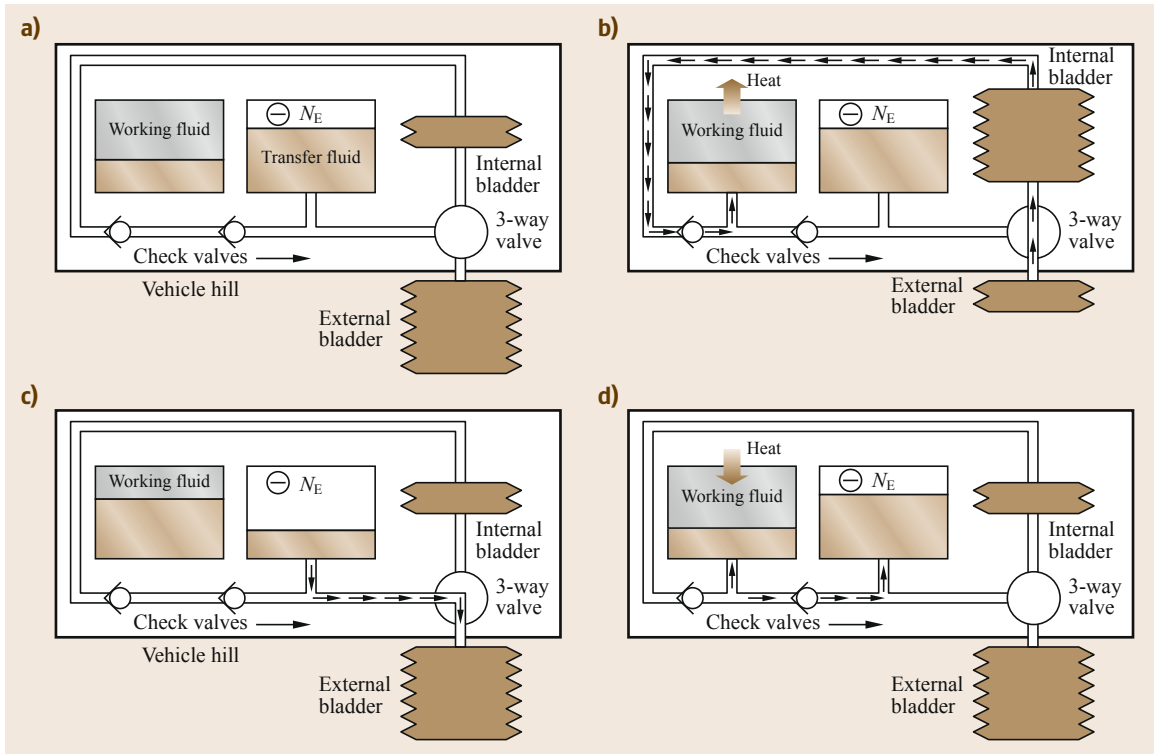


Fig. 12.19a–d Thermodynamic cycle of the thermal glider heat pump: (a) at surface in thermal equilibrium, (b) descending, evacuating external bladder and pumping into hull, pressurizing hydraulic accumulator (c), at depth, working fluid frozen and beginning ascent by releasing pressure from hydraulic accumulator (d) fully developed ascent using thermal expansion of melting working fluid (after [12.4])

energetics and transport economy. To make the transport economy analysis problem tractable, the following assumptions are made regarding a long range, depth unlimited roaming type of application:

- Range = 35 000 km
- Profile depth = 1300 m
- Dive angle = 33° .

The hull weight scales with volume. For thermal engines, the oil required and compensator scale with the drive force required. The drive force (provided by the net buoyancy, B) is a function of the glide angle and is the on-axis component of the buoyancy desired. The payload weight is fixed in the analysis. Energy consumption

is based solely on hotel load, i. e., all propulsion energy is assumed to be harvested from the ocean temperature gradients. As a result, as the mission time decreases with increasing velocity, the onboard energy needed decreases. The volume is calculated for the scaled buoyancy, scaled thermal engines, and scaled oil in bladders and compensator. The velocity is then calculated based on the estimated volume and the C_D . Energy is recalculated based on the new velocity and the volume is re-adjusted. The results of taking these steps are in [12.1].

The NTE figures above for some of the larger thermal glider sizes demonstrate that the thermal glider is capable of transport economies unmatched by any existing man-made flier.

12.6 Discussion and Conclusions

Gliders occupy a unique niche in the universe of autonomous underwater vehicles. They have an intrinsic advantage in transport efficiency over conventional prop-driven AUVs due to the simpler vortex dynam-

ics of a wing compared to a propeller. (Propulsion systems for long-distance persistence found in nature, e.g., birds and marine mammals, are based on wings, not propellers.) Due to a wing's simple vortex dy-

namics, gliders with wings can fly cooperatively with other winged vehicles and structures to further improve transport efficiency, in contrast to prop-driven vehicles. In addition, gliders are capable of readily operating throughout their full speed regime, from top sprint speed to creeping flight to free-drifting at neutral buoyancy in which no propulsion energy is consumed. Consequently, gliders offer a persistent, high-endurance solution for many ocean sampling and surveillance missions. Buoyancy-driven gliders also are silent (acoustically and electromagnetically) throughout most of the dive cycle, including when operating at top sprint speed. They create low levels of self-noise for a few percent of the total dive time due primarily to buoyancy engine operation. However, gliders are generally slower than prop-driven AUVs, typically operating in the speed regime below 3 kts. (Much of a glider's on-station persistence is attributable to these low operating speeds.) In addition, a glider must change depth in order to move forward and so is incapable of level flight. On the other hand, these depth changes allow vertical profiles of ocean properties to be collected and for energy to be extracted from the temperature gradients in the ocean.

In addition to being slower and an inability to conduct level flight, gliders are less maneuverable and more balance sensitive than prop-driven AUVs. However, possibly the greatest disadvantage is the additional vehicle interior volume consumed by, and the additional complexity of, a buoyancy engine compared to a prop-driven system.

The calculus of gliding has been explored for ways of increasing the horizontal point-to-point transport efficiency and speed of underwater gliders. An analytic solution for the minimum specific energy consumption (maximum L/D) indicates that increasing the net buoyancy volume of the vehicle V_b increases the speed as $\sqrt{V_b}$ while specific energy consumption E_e declines as $E_e \approx V_b^{-\xi/4}$, where $1/5 \leq \xi \leq 1/2$. Since buoyancy engine capacity is some fraction n_b of vehicle volume, V_0 , this finding immediately argues for larger gliders for

improved horizontal transport efficiency. The challenge therefore reduces to finding the most efficient geometries for large volumes. Of all the geometric properties of the glider, the wetted surface to wing area ratio, $N_A = A_t/A_0$, has the strongest influence on specific energy consumption, with E_e decreasing as $E_e \approx N_A^{1/2}$ with decreasing N_A . The flying wing glider offers a 9-fold reduction in the wetted surface to wing area ratio over existing profiling gliders, which offsets the 3-fold (at most) increase in profile drag resulting from the thick wing section of a flying wing. The other benefit derived from concentrating the vehicle volume in the wing is that a large wing area reduces the magnitudes of lift coefficient C_L required to support a given V_b , thereby reducing the associated induced drag, the largest component of drag at maximum L/D . However, increasing wing area indefinitely becomes mutually exclusive with high aspect ratio, $N_R = S^2/A_0$, where S is the wingspan. Specific energy consumption was shown to decline with decreases in the ratio of induced drag factors at a rate given by $E_e \approx C_L^{\xi/4} / N_R^{(1/2-\xi/4)}$.

Other factors that favor flying wing geometries for many classes of underwater gliders are higher Reynolds number on the wing section due to larger wing chord, leading to higher maximum lift-to-drag ratios and avoidance of rapid L/D degradation occurring in the 10^4 Reynolds number regime, and increased structural depth of the center section allowing increases in wingspan (and aspect ratio) with fewer weight penalties compared to winged bodies of revolution [12.31–33]. Analytic and numerical comparisons, supported by at-sea results, for large gliders ($V_0 \approx 1000$ L) of comparable net buoyancy demonstrate that a flying wing glider is about 43% more efficient in horizontal transport, but that a winged body of revolution glider has about a 30% advantage in maximum cross-country speed. All gliders designed for long-duration, long-distance flights certainly would benefit significantly from using a buoyancy engine that can harvest energy from the temperature gradients in the ocean.

References

- | | | | |
|------|---|------|---|
| 12.1 | S. A. Jenkins, D. E. Humphreys, J. Sherman, J. Osse, C. Jones, N. Leonard, J. Graver, R. Bachmayer: <i>Underwater Glider System Study</i> , Scripps Institution of Oceanography, Tech. Rep. 57 (University of California, San Diego, La Jolla 2003) online available at http://repositories.cdlib.org/sio/techreport/53/ | 12.3 | C.C. Eriksen, T.J. Osse, R.D. Light, T. Wen, T.W. Lehman, P.L. Sabin, J.W. Ballard, A.M. Chiodi: Seaglider: A long-range autonomous underwater vehicle for oceanographic research, <i>IEEE J. Ocean. Eng.</i> 26 (4), 424–436 (2001) |
| 12.2 | J. Sherman, R.E. Davis, W.B. Owens, J. Valdes: The autonomous underwater glider spray, <i>IEEE J. Ocean. Eng.</i> 26 (4), 437–446 (2001) | 12.4 | D.C. Webb, P.J. Simonetti, C.P. Jones: SLOCUM: An underwater glider propelled by environmental energy, <i>IEEE J. Ocean. Eng.</i> 26 (4), 447–452 (2001) |
| | | 12.5 | R. H. Oversmith, R. E. Leadon: <i>Concept Whisper: A buoyancy-propelled, multiple cycle under-</i> |

- sea glide vehicle, Tech. Rep. GDI C-62-206A (General Dynamics/Convair, San Diego 1962)
- 12.6 H. Stommel: The SLOCUM mission, *Oceanography* **2**(1), 22–25 (1989)
- 12.7 H. Tennekes: *The Simple Science of Flight* (MIT Press, Cambridge 1997)
- 12.8 C. P. Rains: *Analytical Investigation of the Performance Characteristics of Cyclic Glide Undersea Vehicles*, Tech. Rep. GDI C419-69-006 (General Dynamics Corp., San Diego 1968)
- 12.9 M. Van Dyke: *An Album of Fluid Motion* (Parabolic, Stanford 1982)
- 12.10 T. Bjornstad, NOAA Fisheries, Protected Resource Division, Southwest Fisheries Science Center, https://commons.wikimedia.org/wiki/File:Blue_Whale_001_body_bw.jpg, (2007)
- 12.11 H. Glauert: *Elements of Aerofoil and Aircrew Theory*, 2nd edn. (Cambridge Univ. Press, Cambridge 1948)
- 12.12 J.H. McMasters: An analytic survey of low speed flying devices: Natural and man-made, *Tech. Soar.* **3**(4), 17–42 (1974)
- 12.13 C.J. Pennycuik: Gliding flight of the Fulmar Petrel, *J. Exp. Biol.* **37**, 330–338 (1960)
- 12.14 J.H. McMasters, R.M. Cummings: Airplane design and biomechanics of flight – A more completely multi-disciplinary perspective, AIAA 42nd Aerosp. Sci. Meet. (2004), AIAA2004-532
- 12.15 C.H. Greenewalt: Dimensional relationships for flying animals, *Smithson. Misc. Collect.* **144**, 1–46 (1962)
- 12.16 B.W. McCormick: *Aerodynamics, Aeronautics and Flight Mechanics* (Wiley, New York 1979)
- 12.17 L. Prandtl, O.G. Tietjens: *Applied Hydro- and Aeromechanics* (McGraw-Hill, New York 1934)
- 12.18 S.A. Jenkins, J. Wasyl: Optimization of glides for constant wind fields and course headings, *J. Aircr.* **27**(7), 632–638 (1990)
- 12.19 R. Eppler: Laminarprofile fur Segelflugzeuge, *Z. Flugwiss.* **3**, 346–353 (1955)
- 12.20 D. Althaus: *Stuttgarter Profilkatalog I* (Vieweg, Braunschweig 1981)
- 12.21 S.R. Hoerner: *Fluid Dynamic Drag* (Hoerner Fluid Dynamics, Bakersfield 1965)
- 12.22 F.A. Cleveland: Size effects in conventional aircraft design, *J. Aircr.* **7**(6), 483–511 (1970)
- 12.23 N.K. Delany, N.E. Sorensen: *Low-Speed Drag of Cylinders of Various Shapes*, Tech. Note, Vol. 3038 (NACA, Washington 1953)
- 12.24 H. Schlichting: *Boundary Layer Theory* (McGraw-Hill, New York 1960)
- 12.25 A.L. Bolsunovsky, N.P. Buzoverya, B.I. Gurevich, V.E. Denisov, A.I. Dunaevsky, L.M. Shkadov, O.V. Sonin, A.J. Udzhuhu, J.P. Zhurihin: Flying wing – Problems and decisions, *Aircr. Des.* **4**, 193–219 (2001)
- 12.26 V.E. Denisov, A.L. Bolsunovsky, N.P. Buzoverya, B.I. Gurevich: Recent investigations of the very large passenger blended-wing-body aircraft, *Proc. Int. Conf. Acoust. Speech*, Vol. 98 (1998), paper 98-4.10.3
- 12.27 COSMOS (FlowWorks, Los Angeles 2001)
- 12.28 R.F. Stengel: *Flight Dynamics* (Princeton Univ. Press, Princeton 2004)
- 12.29 J.G. Graver, R. Bachmayer, N.E. Leonard: *ONR Underwater Glider Systems Study Glider Design Notes, Part 1*, Tech. Rep. (Princeton Univ., Princeton 2003)
- 12.30 H. Reichmann, P. Lert: *Cross-Country Soaring* (Thomson, Santa Monica 1978)
- 12.31 R. Horten: Toward the theory of flying wings, http://www.nurflugel.com/Nurflugel/Horten_Nurflugels/horten_nurflugels.html (2008) translated by Y. Leshinski
- 12.32 J. K. Northrop: The development of all-wing aircraft, *Roy. Aeronaut. Soc.* **51**, 481–510 (1947) 35th Wilbur Wright Memorial Lecture
- 12.33 J.H. McMasters, I.M. Kroo: Advanced configurations for very large transport airplanes, *Aircr. Des.* **1**(4), 217–242 (1998)